Elastic Properties of Model Porous Ceramics

by

Anthony P. Roberts
Centre for Microscopy and Microanalysis
University of Queensland
St. Lucia, Queensland 4072 Australia

and

Edward J. Garboczi
Building and Fire Research Laboratory
National Institute of Standards and Technology
Gaithersburg, MD 20899 USA

Reprinted from Journal of the American Ceramic Society, Vol. 83, No. 12, 3041-3048, 2000.

NIST
National Institute of Standards and Technology
Technology Administration, U.S. Department of Commerce

journal

J. Am. Ceram. Soc., 83 [12] 3041–48 (2000)

Elastic Properties of Model Porous Ceramics

Anthony P. Roberts[†,‡] and Edward J. Garboczi[*,†]

Building Materials Division, National Institute of Standards and Technology, Gaithersburg, Maryland 20899, and Centre for Microscopy and Microanalysis, University of Queensland, St. Lucia, Queensland 4072, Australia

The finite-element method (FEM) is used to study the influence of porosity and pore shape on the elastic properties of model porous ceramics. Young's modulus of each model is practically independent of the solid Poisson's ratio. At a sufficiently high porosity, Poisson's ratio of the porous models converges to a fixed value independent of the solid Poisson's ratio. Young's modulus of the models is in good agreement with experimental data. We provide simple formulas that can be used to predict the elastic properties of ceramics and allow the accurate interpretation of empirical property–porosity relations in terms of pore shape and structure.

I. Introduction

The elastic properties of two-phase (solid–pore) porous materials depend on the geometrical nature of the pore space and solid phase as well as the value of porosity.[1–4] Relevant aspects of porous materials may include pore shape and size as well as the size and type of the interconnections between solid regions. These features, which generally lack precise definition, comprise the microstructure of the material. To predict properties or properly interpret experimental property–porosity relationships, it is necessary to have an accurate method of relating elastic properties to porosity and microstructure. In this paper we use the finite-element method (FEM) to derive simple formulas that relate Young's modulus and Poisson's ratio to porosity and microstructure for three different models of microstructure.

There have been several different methods to deriving property–porosity relations for porous materials. Formulas derived using the *micromechanics* method[5–7] are essentially various methods of approximately extending exact results for small fractions of spherical or ellipsoidal pores to higher porosities. This includes the differential[8] and self-consistent methods[9–12] as well as the commonly used semiempirical correction to the dilute result made by Coble and Kingery[1] to explain the properties of porous alumina. A drawback of this approach is that the microstructure corresponding to a particular formula is not precisely known; hence, agreement or disagreement with data can neither confirm nor reject a particular model. Another problem is that these types of models provide no predictions for the case where the microstructure is comprised of incompletely sintered grains, which is a common morphology in porous ceramics. Another method[3,13] uses *minimum solid area* (MSA) models. In this method purely geometrical reasoning is used to predict the elastic moduli based on the weakest points within the structure. Again, the microstructure that corresponds to the MSA predictions is not exactly known. Semiempirical relations[2] generally provide a reasonable means of describing data, extrapolating results, and comparing data among materials. However, because they lack a rigorous connection with microstructure, these results offer neither predictive nor interpretive power. Theoretical bounds[5,14] exist for the elastic properties, but the vanishing of the lower bound for porous materials lessens their predictive power when the upper bound does not provide a good estimate. There are other approaches, including the generalized method of cells.[4,6]

Another method is to computationally solve the equations of elasticity for digital models of microstructure.[15,16] In principle this can be done exactly. However, large statistical variations and insufficient resolution have limited the accuracy of results obtained to date. Only recently have computers been able to handle the large three-dimensional models and number of computations needed to obtain reasonable results. As input to the method, we use three different microstructural models that broadly cover the types of morphology observed in porous ceramics. The models are based on randomly placed spherical pores, solid spheres, and ellipsoidal pores.[14] The centers of the pores or solid particles are uncorrelated, which leads to realistic microstructures in which both the pore and solid phase are interconnected. The results, which can be expressed simply by two- (or sometimes three-) parameter relations, correspond to a particular microstructure and explicitly show how the properties depend on the nature of the porosity. Therefore, the results can be used as a predictive tool for cases where the microstructure of the ceramic is similar to one of the models and as an interpretive tool if the microstructure is unknown. The numerically exact FEM results are compared with various well-known micromechanics and MSA results to determine how close an approximation a particular formula provides for each model. In the FEM, we can freely vary the properties of the solid phase, allowing us to determine the dependence of Young's modulus and Poisson's ratio on the solid Poisson's ratio as well as on the porosity. This question has attracted recent interest in the ceramics literature.[17–19]

II. Computational Results

A microstructure made up of a digital image is already naturally discretized and, therefore, lends itself to numerical computation of many quantities. FEM uses a variational formulation of the linear elastic equations and finds the solution by minimizing the elastic energy via a fast conjugate gradient method. The digital image is assumed to have periodic boundary conditions. Details of the theory and programs used are reported in the papers of Garboczi and Day[15] and Garboczi.[20]

To obtain accurate results using FEM on models of random porous materials, it is absolutely necessary to estimate and minimize three sources of error: finite size effects, discretization errors, and statistical fluctuations. This generally has not been done in the past because of limitations in computer memory and speed. FEM results for random microstructures do not have much meaning without such an error analysis.

The various sources of error are defined in the following way. The length scale of the microstructure is fixed, usually by fixing

G. W. Scherer—contributing editor

Manuscript No. 188868. Received December 16, 1999; approved June 28, 2000.
Supported by the Fulbright Foundation, the Australian Research Council, and the Partnership for High-Performance Concrete Technology program of the National Institute of Standards and Technology.
*Member, American Ceramic Society.
†National Institute of Standards and Technology.
‡University of Queensland.

the size of a typical pore (e.g., the spherical pore radius). The size of the system is then controlled by the side length of the cubic sample, denoted T. The size of T compared to the pore size controls how many pores appear in the computational cell. A real material has many thousands or more such pores. Errors can occur in using a smaller number in a periodic cell to simulate a much larger number. We vary T to map this effect.

Once a value of T is chosen that minimizes finite size errors but is computationally possible, we next must consider the discretization error, which comes about because we are using discrete pixels to represent continuum objects. The number of pixels along each edge of the cubical unit cell is M, giving a resolution of $dx = T/M$ (in units of micrometers per pixel, if T is in micrometers). For the chosen value of T, a value of M is chosen that also gives acceptable discretization errors, usually on the order of a few percent.

Finally, when computing the properties of random materials, either computationally or experimentally, we must carefully choose the number of samples (N_s) over which the results need to be averaged to produce acceptable uncertainties. This value is again chosen, within computational constraints, to keep statistical fluctuations within a few percent.

(1) Overlapping Solid Spheres

Realizations of the overlapping solid-sphere model[14,21] are generated by placing solid spheres at random points in the unit cell. This produces a set of overlapping grains that mimic the microstructure of sintered ceramic composites (see Fig. 1(a)). The space outside the solid grains is the pore space, with porosity ϕ. The pore phase is macroscopically connected when ϕ is greater than ~0.03, and the solid phase remains connected for ϕ less than ~0.7.[14] When $\phi > 0.7$, the solid phase is composed of isolated solid particles. Therefore, between $\phi = 0.03$ and $\phi = 0.7$, the overlapping solid-sphere model is bicontinuous. In ceramics, generally, $\phi < 0.4$ in this bicontinuous regime. Therefore, we consider the elastic properties for $0.1 \leq \phi \leq 0.5$, where the solid Poisson's ratio (ν_s) varies over the range $0.1 \leq \nu_s \leq 0.4$.

To generate the microstructure, we choose solid spheres of radius $r = 1$ μm. The elastic properties are length-scale invariant; therefore, the results apply to spheres of any radius for which the continuum assumption holds. A preliminary study has shown that finite size errors are acceptably small for cubic samples with $T = 12$ μm. To study the discretization errors we have generated one realization of the model with $\phi = 0.5$ at $M = 48$–128. The elastic properties depend quite strongly on resolution. We have found that the variation of Young's modulus with M can be described by the relation[22]

$$E_{FEM}(M) \approx E_0 + aM^{-1} \tag{1}$$

where E_0 is the continuum value (corresponding to infinitely large M). The same is true for Poisson's ratio. Even at $M = 128$ the finite-element code overestimates the "exact" result for Young's modulus by 30%. Therefore, for the overlapping sphere model, it is necessary to measure the elastic moduli at three different values of M and extrapolate the results to $M \to \infty$. We choose $N_s = 5$ samples at each resolution and porosity, except at $\phi = 0.5$, where large statistical variations imply that more samples are necessary (i.e., $N_s = 10$). Thus, 30 different realizations of the models are considered, each at three different discretizations, for a total of 90 models.

The statistical variations in Young's modulus and Poisson's ratio for the case $\nu_s = 0.2$ are shown in Table I. The error bars shown in Table I are equal to twice the standard error (SE = $\sigma/N_s^{1/2}$, with σ the standard deviation). Therefore, there is a 95% chance that the "true" result lies between the indicated error bars. The results are accurate to within 20% at $\phi = 0.5$; the error decreases with porosity to <10% for $\phi \leq 0.3$. The expected Gaussian distribution of the measured averages implies that the results are actually more accurate than this. For example, the anticipated relative errors are halved if a 68% likelihood threshold is used (i.e., ± one standard error).

In addition to the above results, we also have computed the elastic moduli of the 90 model microstructures at solid Poisson's ratios of 0.1, 0.3, and 0.4. The statistical variation is not significantly different from the case $\nu_s = 0.2$. Combined with the data for $\nu_s = 0.2$, this covers most commonly occurring solids. The scaled Young's modulus for each value of ν_s is plotted against porosity in Fig. 2. Remarkably, the scaled Young's modulus of the porous material appears to be practically independent of ν_s. This result has been proved to be exact in two dimensions[23,24] and appears to hold to a very good approximation in three dimensions. We have found that Young's modulus data are well described by an equation of the form

$$\frac{E}{E_s} = \left(1 - \frac{\phi}{\phi_0}\right)^n \tag{2}$$

where $n = 2.23$, $\phi_0 = 0.652$, and $0 \leq \phi \leq 0.5$. n and ϕ_0 are empirical correlation parameters and should not be interpreted as the percolation exponent and threshold, respectively. Percolation concepts are generally valid closer to the threshold $\phi_c \approx 0.7$ (for this model), and a higher value of n is expected. The computational cost of accurately measuring the elastic properties increases greatly as the percolation threshold is approached.

Poisson's ratio of the porous material is shown in Fig. 3 as a function of ϕ and ν_s. Figure 3 appears to be a flow diagram,[23] where Poisson's ratio asymptotically approaches a fixed point, independently of the value of the solid Poisson's ratio. This flow diagram has been analytically proved to hold in two dimensions, when a percolation threshold exists at which Young's modulus goes to zero.[23,24] This flow diagram also appears to be valid in three dimensions as well, within numerical uncertainty. Poisson's ratio data shown in Fig. 3 can be roughly described by the simple linear relation,

$$\nu = \nu_s + \frac{\phi}{\phi_0}(\nu_0 - \nu_s) = \nu_0 + \left(1 - \frac{\phi}{\phi_0}\right)(\nu_s - \nu_0) \tag{3}$$

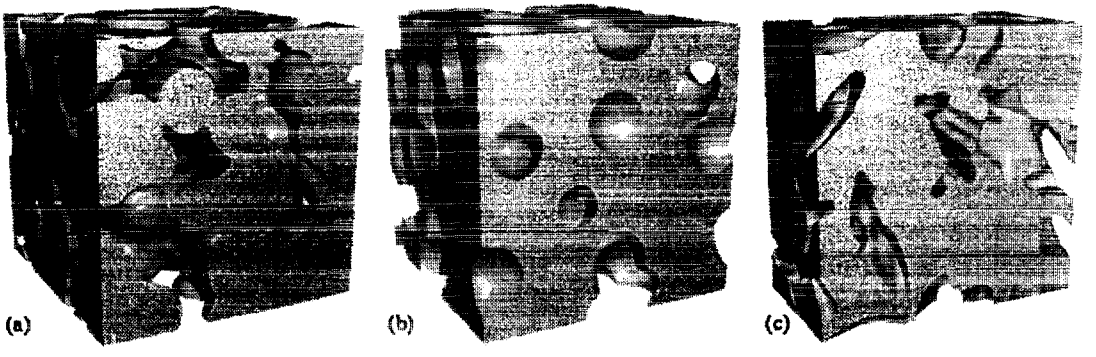

Fig. 1. Pieces of the various models studied: (a) overlapping solid spheres, (b) overlapping spherical pores, and (c) overlapping ellipsoidal pores.

Table I. Elastic Properties of the Three Models ($\nu_s = 0.2$)

ϕ	Overlapping solid spheres		Overlapping spherical pores		Overlapping ellipsoidal pores	
	E/E_s	ν	E/E_s	ν	E/E_s	ν
0.1	0.71 ± 1%	0.19 ± 1%	0.80 ± 1%	0.20 ± 1%	0.73 ± 2%	0.19 ± 3%
0.2	0.47 ± 2%	0.18 ± 4%	0.62 ± 2%	0.20 ± 2%	0.52 ± 3%	0.18 ± 4%
0.3	0.25 ± 6%	0.17 ± 9%	0.46 ± 3%	0.21 ± 3%	0.34 ± 4%	0.18 ± 6%
0.4	0.12 ± 13%	0.15 ± 25%	0.33 ± 4%	0.21 ± 4%	0.20 ± 3%	0.18 ± 4%
0.5	0.039 ± 22%	0.15 ± 21%	0.21 ± 8%	0.22 ± 9%	0.11 ± 4%	0.18 ± 6%

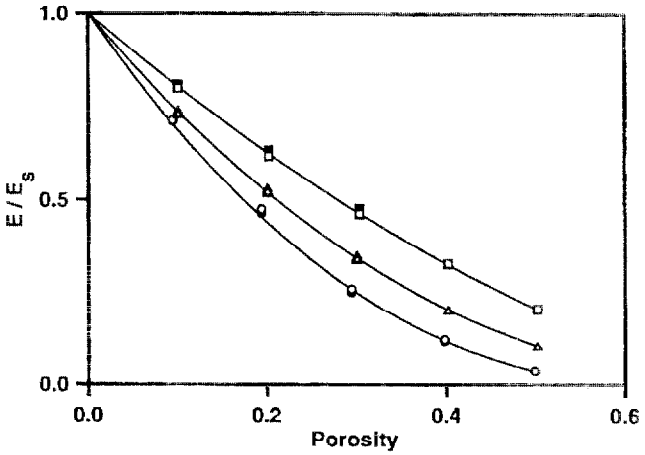

Fig. 2. Young's modulus of the three microstructure models ((—) empirical fits to the equation $E/E_s = (1 - \phi/\phi_0)^n$). Data are shown for (○) overlapping solid spheres ($n = 2.23$, $\phi_0 = 0.652$), (□) spherical pores ($n = 1.65$, $\phi_0 = 0.818$), and (△) ellipsoidal pores ($n = 2.25$, $\phi_0 = 0.798$) for $\nu_s = -0.1, \ldots, 0.4$. E is practically independent of the solid Poisson's ratio in each case (the various values of $E(\nu_s)$ at each porosity are almost indistinguishable).

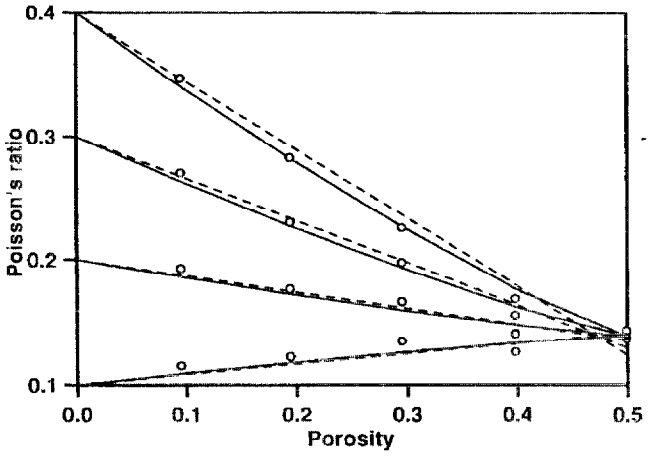

Fig. 3. Poisson's ratio of the overlapping solid-sphere model as a function of porosity for $\nu_s = 0.1$–0.4 ((– – –) empirical fit to Eq. (3), (—) three-parameter relation given in Eq. (4), with the value of all parameters given in the text). Intercepts of the lines at zero porosity correspond to the solid Poisson's ratio.

with two fitting parameters $\nu_0 = 0.140$ and $\phi_0 = 0.472$. A more accurate fit is obtained with the three-parameter relation,

$$\nu = \nu_0 + \left(1 - \frac{\phi}{\phi_0}\right)^m (\nu_s - \nu_0) \tag{4}$$

with $\nu_0 = 0.140$, $\phi_0 = 0.500$, and $m = 1.22$.

(2) Overlapping Spherical Pores

The overlapping spherical pore (or swiss cheese) model[14,21] is generated by interchanging the roles of the solid and pore phase of the overlapping solid-sphere model (see Fig. 1(b)). The morphology corresponds to isolated spherical pores at low porosity, with the pores becoming macroscopically interconnected at $\phi \approx 0.3$. The solid phase remains connected up to $\phi \approx 0.97$. This type of morphology can occur in ceramics generated with a particulate filler[1] or where bubbles form in a molten state.[25] We consider solid Poisson's ratios in the range $-0.1 \leq \nu_s \leq 0.4$.

We have determined that statistical errors are acceptable for a computational cube of size $T = 12$ μm with pores of $r = 1$ μm. When we use $M = 80$ pixels, the discretization errors are <3% for $\phi = 0.5$ and <2% for $\phi = 0.3$. Therefore, it is not considered necessary to generate samples at different discretizations (M) and extrapolate the results. As for solid spheres, Young's modulus is independent of the solid Poisson's ratio to a very good approximation. Young's modulus can be described by Eq. (2) with $n = 1.65$ and $\phi_0 = 0.818$ (Fig. 2). Poisson's ratio of the porous material is shown in Fig. 4 and is simply described by the linear relation given in Eq. (3) with $\nu_0 = 0.221$ and $\phi_0 = 0.840$. Again, a flow diagram is observed.

(3) Overlapping Ellipsoidal Pores

A common method of analyzing the effect of pore shape on elastic properties is to study ellipsoidal pores. In analytic formulas, it is possible to treat the limiting cases of needles and platelets, although the difficulty of resolving these fine structures prohibits these limits from being treated with FEM. However, the percolation properties of these limiting cases can be computationally studied.[26] To gauge the effect of deviations from spherical-shaped pores, we considered isotropically oriented overlapping oblate ellipsoidal pores bounded by the surface $(x/a)^2 + (y/b)^2 + (z/c)^2 = 1$ with $a = b = 1$ μm and $c = 0.25$ μm (see Fig. 1(c)). For this case, the pore phase becomes connected at $\phi = 0.2$.[26] Statistical errors have been found to be acceptable for a computational cube of size $T = 10$ μm. When $M = 96$ pixels is used, the discretization errors are 3% for $\phi = 0.5$ and 2% for $\phi = 0.3$. As

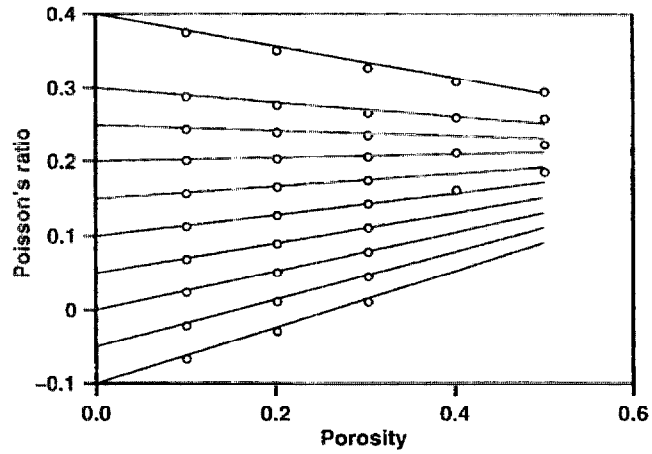

Fig. 4. Poisson's ratio of the overlapping spherical pore model as a function of the solid Poisson's ratio and porosity. Lines are an empirical fit to the relation $\nu = \nu_s + (\phi/\phi_0)(\nu_0 - \nu_s)$, with $\nu_0 = 0.221$ and $\phi_0 = 0.840$. Intercepts of the lines at zero porosity correspond to the solid Poisson's ratio.

for the case of spherical pores, these errors are considered sufficiently small; therefore, the added computational burden of the extrapolation technique can be again avoided.

Again Young's modulus has been found to be independent of the solid Poisson's ratio to a very good approximation. The results, shown in Fig. 2, can be accurately described by Eq. (2) with $n = 2.25$ and $\phi_0 = 0.798$. Poisson's ratio (Fig. 5) can be fitted roughly using Eq. (3) with $\nu_0 = 0.166$ and $\phi_0 = 0.604$. A better fit is obtained using Eq. (4) with $m = 1.91$, $\nu_0 = 0.161$, and $\phi_0 = 0.959$. A flow diagram similar to that shown before is obtained.

The central processing unit (CPU) time and memory required for these computations are an important "experimental" detail. The memory requirement for a given model is $230M^3$ bytes, where M is the edge length in pixels of a cubic unit cell. Therefore, for the largest computations conducted, $M = 128$, the memory requirement is ~500 Mbytes. The amount of CPU time consumed is ~3000 h, divided among different modern workstations.

III. Comparison with Micromechanical and MSA Formulas

In this section we compare a selection of well-known theoretical results with the "numerically exact" data computed in the previous section. These results include analytically exact results (bounds, expansions, dilute limits, and composite sphere assemblage) and approximate results (effective medium theories and minimum solid area models).

There are several types of exact bounds that have been derived for elastic materials.[5,14] These are equations involving the various phase moduli, the volume fractions of the various phases, and various correlation functions that define the geometry of the composite. The upper bound gives the maximum possible composite elastic moduli, and the lower bound gives the minimum possible composite elastic moduli. The bounds used in this paper are three-point bounds, which have been written out explicitly for overlapping solid spheres and overlapping spherical pores.[14] In the case where one phase has zero elastic moduli, as is true in this paper, the lower bound becomes zero as well, and, therefore, only the upper bound is meaningful.

An exact perturbation expansion also exists, where the elastic moduli of a two-phase material are expanded in terms of parameters involving the individual elastic moduli of each phase and geometrical quantities.[27,28] This expansion has been performed to three terms explicitly, and it is this truncated form to which we compare our numerical data. The result is expected to be accurate when the void phase is not interconnected.

Another exact result, which is used later in this section to build the various effective medium theories, is the case of dilute spherical pores, for which the exact effective moduli are given by

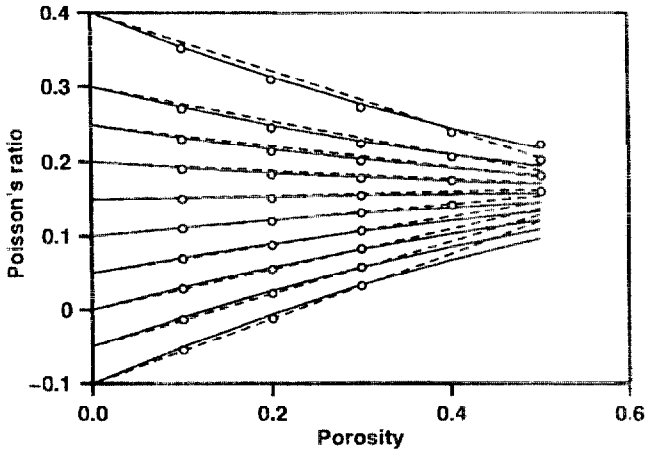

Fig. 5. Poisson's ratio of the overlapping ellipsoidal pore model as a function of the solid Poisson's ratio and porosity ((—) empirical fit to Eq. (4), and (– – –) linear fit to Eq. (3), with $\nu_0 = 0.166$ and $\phi_0 = 0.604$). Intercepts of the lines at zero porosity correspond to the solid Poisson's ratio.

$$K = K_m + c_i P^{mi}(K_i - K_m) \tag{5}$$

$$G = G_m + c_i Q^{mi}(G_i - G_m) \tag{6}$$

where

$$P^{mi} = \frac{3K_m + 4G_m}{3K_i + 4G_m}$$

$$Q^{mi} = \frac{G_m + F_m}{G_i + F_m} \tag{7}$$

$$F_m = \frac{G_m}{6}\frac{9K_m + 8G_m}{K_m + 2G_m}$$

where c_i denotes the concentration (volume fraction) of inclusions and the subscripts i and m on the bulk modulus K and shear modulus G denote the properties of the inclusion and matrix, respectively. The result is attributed to numerous authors.[5] For a porous matrix, $K_i = G_i = 0$, and $\phi = c_i$. The result is strictly valid for small concentrations of inclusions $\phi << 1$ (in practice $\phi < 0.1$). Expressed in terms of the engineering constants for porous inclusions this result becomes

$$E = E_m - \frac{3}{2}\phi E_m \frac{9 - 4\nu_m - 5\nu_m^2}{7 - 5\nu_m} + O(\phi^2) \tag{8}$$

$$\nu = \nu_m - \frac{3}{2}\phi \frac{(5\nu_m - 1)(1 - \nu_m^2)}{7 - 5\nu_m} + O(\phi^2) \tag{9}$$

Our prior statement[29] of Eq. (8) inadvertently omitted the factor $\frac{3}{2}$, although the correct result has been used in the paper. A nonzero quadratic term can be added (as an empirical correction) to ensure that $E = 0$ at $\phi = 1$. This is suggested by Coble and Kingery[1] for MacKenzie's[30] result for spherical pores, which is equivalent to Eqs. (5)–(7) with $K_i = G_i = 0$.

To adapt the dilute formulas to the case of finite porosity, several proposals have been made. The approximate equations that result are usually called effective medium theories. The most common approximation is the so-called self-consistent method (SCM) of Hill[9] and Budiansky.[10] In this model the equations of elasticity are solved for a spherical inclusion embedded in a medium of unknown effective moduli. The effective moduli K and G are then derived. In the dilute case the embedding medium is only the matrix. The Hill–Budiansky result can be stated as[12]

$$c_i P^{*i}(K_i - K_*) + c_m P^{*m}(K_m - K_*) = 0 \tag{10}$$

$$c_i Q^{*i}(G_i - G_*) + c_m Q^{*m}(G_m - G_*) = 0 \tag{11}$$

where K_* and G_* denote the effective moduli and P^{*m} and Q^{*m} are given in Eq. (7). The equations cannot be explicitly solved, and numerical methods are necessary (see Hill[9] and Berryman[12] for details). In the case of porous inclusions, the moduli vanish at $\phi = \frac{1}{2}$, which is a property not shared with most composites (e.g., the overlapping sphere model). To derive a more realistic result, Christensen and Lo[31] have generalized the SCM (GSCM) to the case of a spherical shell embedded in a matrix of unknown moduli. The result is complicated and not reproduced here.

The differential method (reviewed by McLaughlin[8]) provides an alternative model using a similar philosophy. Suppose that the effective moduli of a composite medium are known to be K_* and G_*. If a small additional concentration of inclusions is added, the change in K_* and G_* is approximated to be that which would result if a dilute concentration of inclusions was added to a uniform, homogeneous matrix with moduli K_* and G_*. This leads to a pair of coupled differential equations:

$$\frac{dK_*}{dc_i} = P^{*i}\frac{K_i - K_*}{1 - c_i} \qquad K_*(c_i = 0) = K_m \tag{12}$$

$$\frac{dG_*}{dc_i} = Q^{*i}\frac{G_i - G_*}{1 - c_i} \qquad G_*(c_i = 0) = G_m \tag{13}$$

The dilute result, the self-consistent result,[12] and the differential method[8] can be extended to the case of spheroidal inclusions. The general results[11] for P^{mi} and Q^{mi} have been given by Berryman.[12] In addition to these results, Wu[11] has derived a variant of the self-consistent method, where K_* and G_*, the effective moduli, are found by implicitly solving the equations

$$K_* = K_m + c_i P^{*i}(K_i - K_m) \tag{14}$$

$$G_* = G_m + c_i Q^{*i}(G_i - G_m) \tag{15}$$

A different type of microstructure is provided by the Hashin[5,32] model of space-filling polydisperse hollow spheres (composite-sphere assemblage). Although a simple formula exists for the bulk modulus over the full porosity range,[32] exact results for Young's moduli are not available. Ramakrishnan and Arunachalam[33] recently derived the approximation

$$\frac{E}{E_s} = \frac{(1-\phi)^2}{(1+2\phi-3\nu_s\phi)} \tag{16}$$

$$\nu = \frac{(4\nu_s + 3\phi - 7\nu_s\phi)}{4(1+2\phi-3\nu_s\phi)} \tag{17}$$

However, the derivation is not rigorous. In particular, the exact result for the bulk modulus of the model[32] is about twice that predicted by Eqs. (16) and (17) at $\phi = 0.5$. Because Eq. (16) provides reasonable agreement with experimental data for porous ceramics,[17] we compare its predictions to our FEM data below.

The final class of results we consider is provided by the MSA models[34] (which have been recently reviewed by Rice[3,13]). This approach is based on the assumption that the ratio of the effective moduli to the solid moduli is directly proportional to the minimum ratio of solid contact area to the total cross-sectional area of periodic structures. The approximation derived depends on the particular model considered. We consider two basic models most closely aligned with our FEM data: simple cubic arrays of solid and porous spheres. The latter case provides a particularly simple example of the type of result that can be derived. Suppose the repeat distance of the lattice is $2h$ and the sphere radius is r. Young's modulus is assumed to be proportional to the area fraction, giving

$$\frac{E}{E_s} = \frac{(2h)^2 - \pi r^2}{(2h)^2} = 1 - \frac{\pi}{4}\left(\frac{6}{\pi}\right)^{2/3}\phi^{2/3} \tag{18}$$

because $\phi = \frac{1}{6}\pi(r/h)^3$. The form of the result changes for $r > h$ (or $\phi > \pi/6 = 0.52$) as the spheres begin to coalesce. Rice[3] has reported that the moduli of many different periodic structures can be approximated by the form $E/E_s = e^{-b\phi}$ over a range of porosities: for example, $b \approx 5$ for the solid-sphere model, and $b \approx 3$ for the porous-sphere model. It is argued that, for a given set of data, b can be compared with known values to assess the type of porosity. Often fractions of different types of porosity are assumed to match experimental data, making the method an interpretive rather than a predictive tool. Because we have measured E for microstructures based on solid-sphere contacts and porous spheres, we should be able to ascertain the accuracy of the MSA formulas for these cases.

Figure 6 shows the comparison between the exact three-point bounds[14] for the overlapping solid-sphere and spherical pore cases, the truncated expansion[27,28] for the overlapping spherical pore case, and the numerical results. Clearly, the expansion does better than the three-point bound for the overlapping spherical pore case, although both formulas are fairly close to the numerical results. The bound lies far above the overlapping solid-sphere numerical results, however. For this case, the truncated expansion does not exist. Only the $\nu_s = 0.2$ data are shown. Using the truncated expansion, it can be shown that, in three dimensions, Young's modulus is not exactly independent of the solid Poisson's ratio but is, rather, a very good approximation, as was shown earlier in this paper.

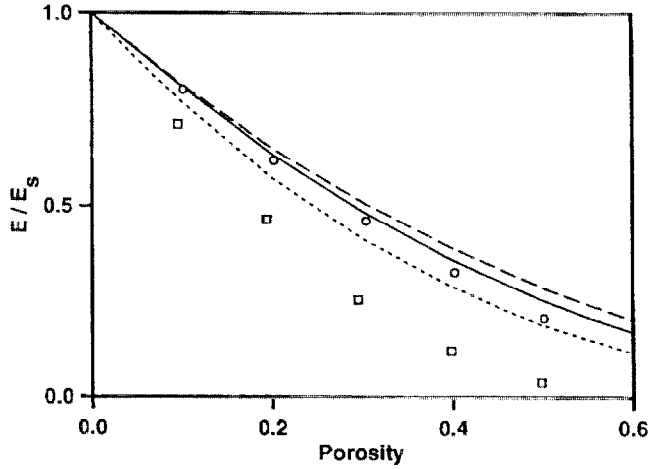

Fig. 6. Comparison of rigorous bounds and expansions to the FEM data for (○) overlapping spherical pores and (□) overlapping solid spheres ((—) truncated expansion and (– – –) three-point upper bound are shown for the spherical-pore case; only the (· · ·) three-point bound is shown for the solid-sphere case; three-point lower bound is zero for porous materials). Poisson's ratio is 0.2 for all the results.

In Fig. 7, we compare the FEM data ($\nu_s = 0.2$) for overlapping spherical pores with dilute and effective medium theory analytic results. At this Poisson's ratio, the SCM and dilute results reduce to $E/E_s = 1 - 2\phi$, whereas the differential and dilute results with the Coble–Kingery correction reduce to $E/E_s = (1-\phi)^2$. Because the analytic results are based on the case of dilute spherical pores, they all match the FEM data at $\phi = 0.1$. The dilute and SCM results underestimate the FEM data at higher porosities because of the aphysical percolation threshold at $\phi = \frac{1}{2}$. The generalized SCM overestimates the data, whereas the differential method performs reasonably well over the entire porosity range. The latter observation might have been anticipated given the close association between the definition of the spherical-pore model and the assumption of the differential method. At increasing porosities we are simply adding additional spherical pores to a porous matrix. The data for overlapping solid spheres are also shown in Fig. 7, and seem to be quite different from any of the available results. This demonstrates that microstructure (the geometrical nature of the porosity) is an important factor besides the actual value of the porosity.

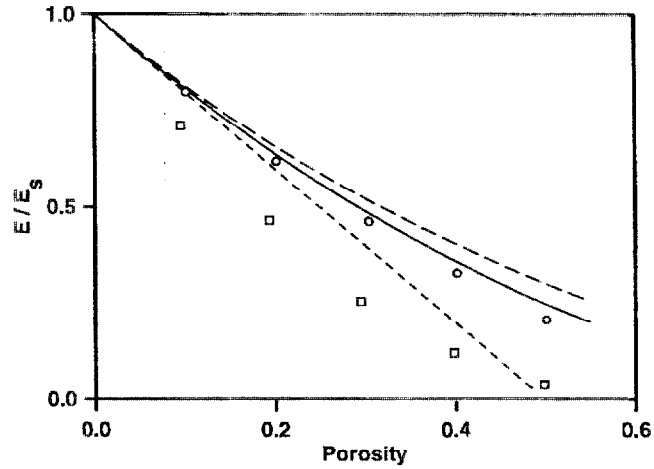

Fig. 7. Comparison of various theories to the FEM data for (○) overlapping spherical pores. Lines correspond to the dilute (– – –) result and self-consistent method[9,10] (or SCM), (—) differential method[8] and dilute result with Coble–Kingery correction, and (– – –) the generalized SCM[31]). Data for the (□) overlapping solid-sphere model (for which no rigorous theories exist) are also shown.

In Fig. 8, the MSA models and the Ramakrishnan and Arunachalam results[33] are compared with the data. The MSA model for spherical pores performs reasonably well, although underestimating the FEM data for overlapping random spherical pores at low porosities ($\phi < 0.3$). The MSA model for solid spheres considerably underestimates these data for $\phi < 0.3$. The Ramakrishnan and Arunachalam[33] approximation falls between the FEM data for $\phi > 0.1$, indicating that it corresponds to neither of the microstructures. For purposes of comparison, we also report numerical results obtained using the computational generalized method of cells[4] For a periodic spherical pore, the results significantly underestimate the FEM data for overlapping spherical pores at low porosities (and, hence, the exact dilute result). It is not clear if this is due to the assumptions or the particular implementation of the method.

The FEM data for overlapping oblate ellipsoidal pores is compared with the available theories in Fig. 9. The SCM results of Wu[11] and Berryman[12] underestimate the porosity as a result of underestimating the physical percolation threshold. The Berryman result performs significantly better than does the Wu result. As for the case of spheres, the differential method matches the data quite closely because of the similarity between the assumptions of the theory and the definition of the model.

We have also compared Poisson's ratio predicted by the various self-consistent and differential methods to the FEM data for overlapping spherical and ellipsoidal pores. The theoretical results converge to different fixed points (e.g., Fig. 3) in qualitative agreement with the data. However, only the differential method provides reasonable agreement with the FEM data (with absolute error <0.02 for $\phi \leq 0.4$ and $0.1 \leq \nu_s \leq 0.4$).

IV. Comparison with Experiment

We now use the FEM results to analyze experimental measurements of the elastic properties of porous ceramic materials. The dependence of the elastic moduli on porosity has been the subject of many studies.[13,17,18] Data for porous alumina from numerous studies[35] are shown in Fig. 10. The Coble–Kingery[1] material is markedly stiffer than other materials, which is in very good agreement with the FEM results for the overlapping spherical pore model. The pores in the alumina matrix are actually created by the incorporation of a particulate filler,[1] which corresponds well with the definition of the model microstructure. The remaining data closely follow the overlapping solid-sphere FEM result for $\phi < 0.25$, indicating that the solid alumina phase has the sintered granular morphology exhibited by the model microstructure (Fig. 1(a)). However, Knudsen reports that several of the samples summarized were also created using particulate fillers. At higher porosities, the solid-sphere result underestimates the data. One reason for this might be that the model contains isolated solid spheres that artificially decrease the actual porosity. This has been checked and found not to be the case for the porosities studied. Therefore, the solid connections in these samples of porous alumina are likely stiffer than those found in the solid-sphere model at $\phi > 0.25$. Overlapping spheres can create very sharp "valleys" between a pair of overlapping solid spheres (see Fig. 1(a)), which would be rounded off in the sintering process, presumably strengthening the solid–solid connection.

Hunter and co-workers[36–39] have studied Young's modulus of several oxides. In all cases, the porous material has been created by sintering a powder of the pure oxide. The results for Young's modulus are reproduced in Fig. 11. For low porosities ($\phi < 0.1$), all of the data follow the FEM results for overlapping spherical pores. For Gd_2O_3, the FEM result continues to provide excellent agreement up to the maximum porosity measured ($\phi = 0.4$), indicating that the microstructure is similar to that of the model (overlapping pores). In contrast, the data for the other three oxides decrease toward the result for overlapping solid spheres, indicating a more granular character.

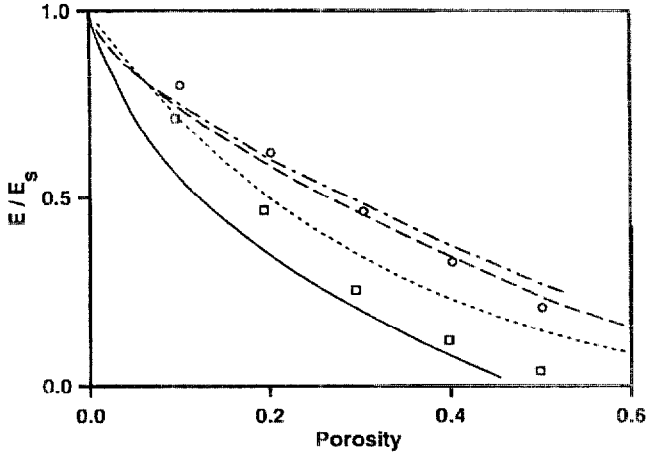

Fig. 8. Comparison of the MSA models[3] to the FEM data for (○) overlapping spherical pores and (□) solid spheres. The (—) MSA solid-sphere model and (– – –) MSA porous sphere model (in simple cubic packings) underestimate the data for low porosities ($\phi < 0.3$); (· · ·) formula of Ramakrishnan and Arunachalam[33] $E/E_s = (1 - \phi)^2/(1 + 1.4\phi)$ and (– · –) results of the generalized method of cells for a periodic spherical pore[4] are also shown.

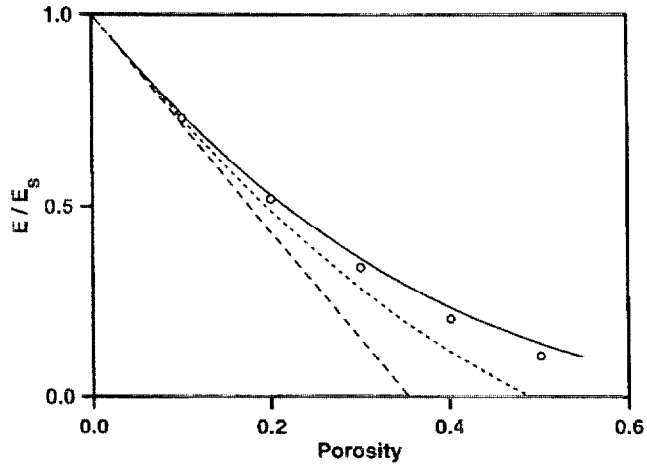

Fig. 9. Comparison of various theories to the FEM data for (○) overlapping oblate ellipsoidal pores. Lines correspond to the (—) differential method[8] and the self-consistent methods of (– – –) Wu[11] and (· · ·) Berryman.[12]

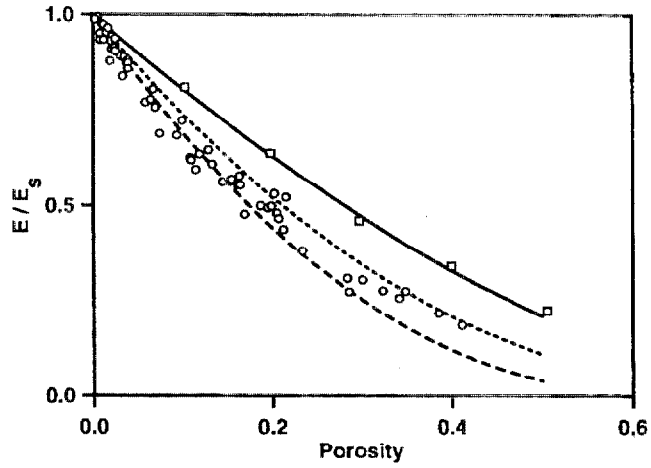

Fig. 10. Data for alumina compiled by (○) Knudsen[35] (E_s = 410 GPa) and by (□) Coble–Kingery[1] (E_s = 386 GPa). Lines correspond to the FEM theories computed in this paper: (—) overlapping spherical pores, (· · ·) overlapping oblate ellipsoidal pores, and (– – –) overlapping solid spheres.

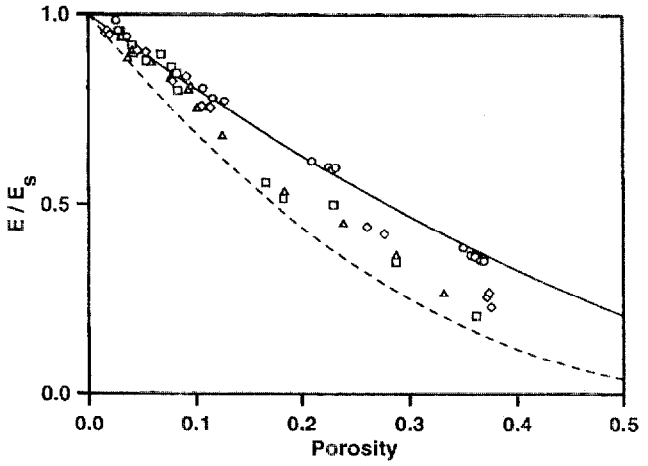

Fig. 11. Data for various oxides measured by Hunter *et al.*[36–39] compared with the FEM theories for (—) overlapping spherical pores and (– – –) overlapping solid spheres ((◇) Sm_2O_3,[36] E_s = 145 GPa; (△) Lu_2O_3,[37] E_s = 193 GPa; (○) Gd_2O_3,[38] E_s = 150 GPa; and (□) HfO_2,[39] E_s = 246 GPa).

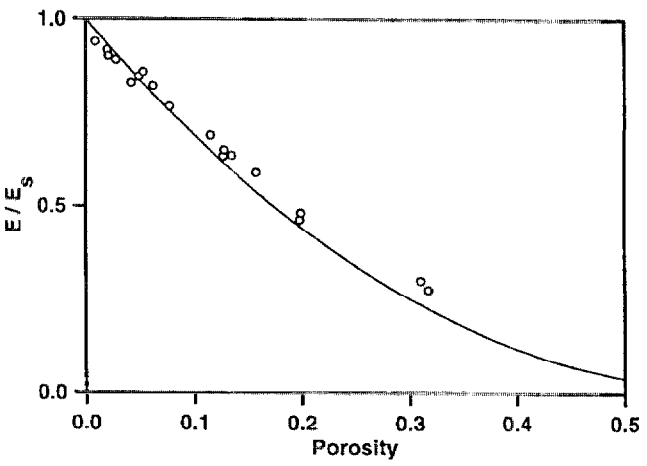

Fig. 13. Data for $MgAl_2O_4$.[40] Value used was $E_s = 41.2 \times 10^6$ psi (284 GPa) indicated on Fig. 3(A) of the reference, rather than the reported value of $E_s = 43.4 \times 10^6$ psi, which appears to be a misprint ((—) corresponds to the FEM theory for overlapping solid spheres).

The data of Walsh *et al.*[25] for porous glass is compared with the FEM results for overlapping spherical pores in Fig. 12. The agreement is good for small to moderate porosities ($\phi < 0.3$), but the FEM results underestimate the data at higher porosities. Walsh *et al.* report that the pores in the glass are actually not interconnected (unlike the overlapping pores of the model). This accounts for the increased stiffness. FEM results begin to deviate from the experimental data at the threshold, where the pores become macroscopically connected ($\phi = 0.3$). Data for sintered $MgAl_2O_4$[40] powder are shown in Fig. 13, and they are well modeled by the FEM results for overlapping solid spheres. Micrographs of the ceramic indicate a granular structure similar to that of the model microstructure (although the grains appear as polyhedra, not spheres).

V. Discussion and Conclusions

We have derived empirical theories for the dependence of Young's modulus on porosity for three distinct models of porous ceramics, based on careful FEM computations. An advantage of these results over many conventional theories is that they correspond to *a priori* known microstructures. The dilute result (extended by Coble–Kingery to all porosities), the differential method, and the self-consistent methods have a built-in microstructure, but, apart from the dilute case, the microstructure is not clear. Therefore, agreement or disagreement with a particular analytic theory neither confirms nor rejects a particular physical model. For the MSA models, the microstructure is exactly known, but the approximation involved in making Young's modulus directly proportional to the contact area leads to a similar conclusion. We have found that the MSA models do not provide quantitative agreement with the moduli of the random microstructures studied. We have found that the differential method (Eqs. (12) and (13)) provides results in reasonable agreement with computed data for the cases of overlapping spherical and ellipsoidal pores, probably because of the similarities between the assumptions of the model and the definitions of the microstructure. Results for the granular model of overlapping solid spheres have not been well modeled by any of the analytic theories, demonstrating the importance of FEM techniques in this case of great physical interest.

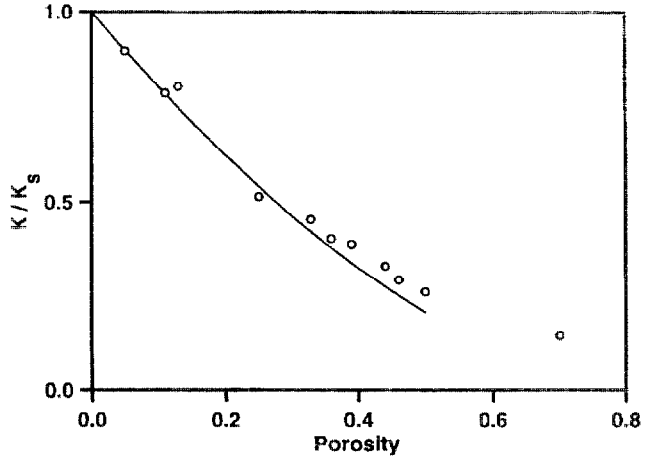

Fig. 12. Data for porous glass[25] (K_s = 46 GPa, ν_s = 0.23) ((—) FEM theory for overlapping spherical pores).

We have also generated data that show the dependence of Poisson's ratio on porosity and the solid Poisson's ratio. It is difficult to study this question experimentally because of the inability to vary Poisson's ratio of the solid independently and the well-known difficulties of accurately measuring Poisson's ratio at moderate to high porosities.[18] At sufficiently high porosities, Poisson's ratio converges to a fixed non-zero value (ν_0), irrespective of the solid Poisson's ratio. For overlapping solid spheres, $\nu_0 = 0.14$; spherical pores, $\nu_0 = 0.22$; and oblate ellipsoidal pores, $\nu_0 = 0.16$. This behavior is exact in two dimensions[23,24] and is exhibited by many of the analytic theories in three dimensions. At present the available experimental data cannot confirm this qualitative behavior.[18] We have shown that Poisson's ratio does not vanish at high porosities, as has been recently argued.[19]

It is not simple to attribute our results to features of the solid-pore morphology—such as the size, shape, distribution, and connectivity of pores or solid grains—because these features have no obvious definition for complex bicontinuous random microstructures. A few general observations can be made and interpreted in terms of interrelated geometrical and mechanical features of the models. For a given porosity, the sintered grain structure of the overlapping solid-sphere model is relatively weak. The small solid contacts between spheres and the highly interconnected porosity (which becomes macroscopically connected at $\phi = 0.03$) lead to a weak structure. We also assume that the valleys that occur between grains provide sites of large stress concentrations and, consequently, large deformations. In contrast, spherical pores provide high (near optimal) stiffness at a given porosity. The dispersed nature of the porosity (which is macroscopically disconnected for $\phi < 0.3$) corresponds to a well-connected solid matrix. Ellipsoidal pores tend to weaken a structure more than spherical pores because of a combination of a less-well-connected solid phase (the pores become macroscopically connected at $\phi = 0.2$) and greater

stresses and deformations near the high-curvature regions of the ellipsoid.

We have compared our FEM results with several sets of previously published experimental data. In cases where the microstructure of the porous ceramics roughly matches that of the models, the agreement is very good. Because the FEM results correspond to a known microstructure, it is possible to explain deviations in terms of specific microstructural features. Thus, comparison of experimental data with the three computational results provides a useful interpretive tool. A given elastic modulus does not correspond to a particular microstructure. Therefore, it is important to corroborate microstructural interpretations obtained from the elastic moduli with information about the particular material (such as a micrograph). In the future, it would be useful to extend this work to higher porosities and to other relevant models (such as nonoverlapping porous spheres). It is also possible to use statistical microstructural information obtained from two-dimensional micrographs to generate models[29] that actually mimic physical microstructures.

References

[1]R. L. Coble and W. D. Kingery, "Effect of Porosity on Physical Properties of Alumina," *J. Am. Ceram. Soc.*, **39** [11] 377–85 (1956).

[2]E. A. Dean and J. A. Lopez, "Empirical Dependence of Elastic Moduli on Porosity for Ceramic Materials," *J. Am. Ceram. Soc.*, **60** [7–8] 345–49 (1977).

[3]R. W. Rice, "Evaluation and Extension of Physical Property–Porosity Models Based on Minimum Solid Area," *J. Mater. Sci.*, **31**, 102–18 (1996).

[4]C. T. Herakovich and S. C. Baxter, "Influence of Pore Geometry on the Effective Response of Porous Media," *J. Mater. Sci.*, **31**, 1595–609 (1999).

[5]Z. Hashin, "Analysis of Composite Materials—A Survey," *J. Appl. Mech.*, **50**, 481–505 (1983).

[6]J. Aboudi, *Mechanics of Composite Materials: A Unified Micromechanical Approach*; pp. 35–109. Elsevier, Amsterdam, the Netherlands, 1991.

[7]R. M. Christensen, *Mechanics of Composite Materials*; pp. 31–72. Wiley, New York, 1979.

[8]R. McLaughlin, "A Study of the Differential Scheme for Composite Materials," *Int. J. Eng. Sci.*, **15**, 237–44 (1977).

[9]R. Hill, "A Self-Consistent Mechanics of Composite Materials," *J. Mech. Phys. Solids*, **13**, 213–22 (1965).

[10]B. Budiansky, "On the Elastic Moduli of Some Heterogeneous Materials," *J. Mech. Phys. Solids*, **13**, 223–27 (1965).

[11]T. T. Wu, "The Effect of Inclusion Shape on the Elastic Moduli of a Two-Phase Material," *Int. J. Solids Struct.*, **2**, 1–8 (1966).

[12]J. G. Berryman, "Long-Wavelength Propagation in Composite Elastic Media II. Ellipsoidal Inclusions," *J. Acoust. Soc. Am.*, **68** [6] 1820–31 (1980).

[13]R. W. Rice, "Comparison of Physical Property–Porosity Behaviour with Minimum Solid Area Models," *J. Mater. Sci.*, **31**, 1509–28 (1996).

[14]S. Torquato, "Random Heterogeneous Media: Microstructure and Improved Bounds on Effective Properties," *Appl. Mech. Rev.*, **44**, 37–76 (1991).

[15]E. J. Garboczi and A. R. Day, "An Algorithm for Computing the Effective Linear Elastic Properties of Heterogeneous Materials: Three-Dimensional Results for Composites with Equal Phase Poisson Ratios," *J. Mech. Phys. Solids*, **43**, 1349–62 (1995).

[16]J. Poutet, D. Manzoni, F. Hage-Chehade, C. G. Jacquin, M. J. Bouteca, J. F. Thovert, and P. M. Adler, "The Effective Mechanical Properties of Random Porous Media," *J. Mech. Phys. Solids*, **44**, 1587–620 (1996).

[17]N. Ramakrishnan and V. S. Arunachalam, "Effective Elastic Moduli of Ceramic Materials," *J. Am. Ceram. Soc.*, **76** [11] 2745–52 (1993).

[18]A. R. Boccaccini, "Comment on 'Effective Elastic Moduli of Ceramic Materials'," *J. Am. Ceram. Soc.*, **76** [10] 2745–52 (1994).

[19]R. W. Rice, "Comment on 'Effective Elastic Moduli of Porous Ceramic Materials'," *J. Am. Ceram. Soc.*, **78** [6] 1711 (1995).

[20]E. J. Garboczi, Internal Rept. No. 6269, National Institute of Standards and Technology, Gaithersburg, MD, 1998; Ch. 2 (available at http://ciks.cbt.nist.gov/garboczi/).

[21]H. L. Weissberg, "Effective Diffusion Coefficient in Porous Media," *J. Appl. Phys.*, **34**, 2636–39 (1963).

[22]A. P. Roberts and M. Teubner, "Transport Properties of Heterogeneous Materials Derived from Gaussian Random Fields: Bounds and Simulation," *Phys. Rev. E: Stat. Phys., Plasmas, Fluids, Relat. Interdiscip. Top.*, **51**, 4141–54 (1995).

[23]A. R. Day, K. A. Snyder, E. J. Garboczi, and M. F. Thorpe, "The Elastic Moduli of Sheet Containing Spherical Holes," *J. Mech. Phys. Solids*, **40**, 1031–51 (1992).

[24]A. V. Cherkaev, K. A. Lurie, and G. W. Milton, "Invariant Properties of the Stress in Plane Elasticity and Equivalence Classes of Composites," *Proc. R. Soc. London, A*, **438**, 519–29 (1992).

[25]J. B. Walsh, W. F. Brace, and A. W. England, "Effect of Porosity on Compressibility of Glass," *J. Am. Ceram. Soc.*, **48** [12] 605–608 (1965).

[26]E. Garboczi, K. Snyder, J. Douglas, and M. Thorpe, "Geometrical Percolation Threshold of Overlapping Ellipsoids," *Phys. Rev. E: Stat. Phys., Plasmas, Fluids, Relat. Interdiscip. Top.*, **52**, 819–28 (1995).

[27]S. Torquato, "Effective Stiffness Tensor of Composite Media—I. Exact Series Expansions," *J. Mech. Phys. Solids*, **45**, 1421–48 (1997).

[28]S. Torquato, "Effective Stiffness Tensor of Composite Media—II. Applications to Isotropic Dispersions," *J. Mech. Phys. Solids*, **46**, 1411–40 (1998).

[29]A. P. Roberts and E. J. Garboczi, "Elastic Properties of a Tungsten–Silver Composite by Reconstruction and Computation," *J. Mech. Phys. Solids*, **47** [10] 2029–55 (1999).

[30]J. F. MacKenzie, "Elastic Constants of a Solid Containing Spherical Holes," *Proc. Phys. Soc. (London)*, **63B** [1] 2–11 (1960).

[31]R. M. Christensen and K. H. Lo, "Solutions for Effective Shear Properties in Three Phase Sphere and Cylinder Models," *J. Mech. Phys. Solids*, **27**, 315–30 (1979).

[32]Z. Hashin, "The Elastic Moduli of Heterogeneous Materials," *ASME J. Appl. Mech.*, **29**, 143–50 (1962).

[33]N. Ramakrishnan and V. S. Arunachalam, "Effective Elastic Moduli of Porous Solids," *J. Mater. Sci.*, **25**, 3930–37 (1990).

[34]F. P. Knudsen, "Dependence of Mechanical Strength of Brittle Polycrystalline Specimens on Porosity and Grain Size," *J. Am. Ceram. Soc.*, **42** [8] 376–87 (1959).

[35]F. P. Knudsen, "Effect of Porosity on Young's Modulus of Alumina," *J. Am. Ceram. Soc.*, **45** [2] 94–95 (1962).

[36]O. Hunter, H. J. Korklan, and R. R. Suchomel, "Elastic Properties of Polycrystalline Monoclinic Sm_2O_3," *J. Am. Ceram. Soc.*, **57** [6] 267–68 (1974).

[37]O. Hunter and G. E. Graddy, "Porosity Dependence of Elastic Properties of Polycrystalline Lu_2O_3," *J. Am. Ceram. Soc.*, **59** [1–2] 82 (1976).

[38]J. A. Haglund and O. Hunter, "Elastic Properties of Polycrystalline Monoclinic Gd_2O_3," *J. Am. Ceram. Soc.*, **56** [6] 327–30 (1973).

[39]S. L. Dole, O. Hunter, and F. W. Calderwood, "Elastic Properties of Stabilized HfO_2 Compositions," *J. Am. Ceram. Soc.*, **63** [3–4] 136–39 (1980).

[40]D. F. Porter, J. S. Reed, and D. Lewis, "Elastic Moduli of Refractory Spinels," *J. Am. Ceram. Soc.*, **60** [7–8] 345–49 (1977). □